

# Load bearing capacity of stainless steel beams at elevated temperatures

## Capacidade resistente de vigas em aço inoxidável a temperaturas elevadas

**Matheus Alves<sup>1</sup> | Luís Mesquita<sup>2</sup> | Paulo Piloto<sup>3</sup> | Nuno Lopes<sup>4</sup> | Flávio Arrais<sup>4</sup> | Paulo Vila Real<sup>4</sup> | Joaquim Pinho-da-Cruz<sup>5</sup>**

<sup>1</sup> Universidade Tecnológica Federal do Paraná, Brasil, [matheusa@alunos.utfpr.edu.br](mailto:matheusa@alunos.utfpr.edu.br)

<sup>2</sup> ISE, Instituto Politécnico de Bragança, Portugal, [lmesquita@ipb.pt](mailto:lmesquita@ipb.pt)

<sup>3</sup> LAETA - INEGI, Instituto Politécnico de Bragança, Portugal, [ppiloto@ipb.pt](mailto:ppiloto@ipb.pt)

<sup>4</sup> RISCO, Universidade de Aveiro, Portugal, [nuno.lopes@ua.pt](mailto:nuno.lopes@ua.pt), [arraais.f@ua.pt](mailto:arraais.f@ua.pt), [pvreal@ua.pt](mailto:pvreal@ua.pt)

<sup>5</sup> TEMA, Universidade de Aveiro, Portugal, [jpc@ua.pt](mailto:jpc@ua.pt)

### abstract

To analyse the load bearing capacity of stainless steel (SS) members at elevated temperatures, a set of three-point bending tests was conducted on RHS 150x100x5 beams with SS grade 1.4301. The numerical modelling of these tests has been performed at elevated temperatures, achieving close approximation to observed experimental results. The load bearing capacity difference between the numerical results and the experimental results is smaller than 10%. Analytical methods were also used to predict the load-deflection behaviour.

**Keywords:** Bending resistance, Stainless steel, Elevated temperatures

### resumo

Para analisar a capacidade portante de elementos estruturais em aço inoxidável a temperaturas elevadas, foi realizado um conjunto de ensaios experimentais à flexão em três pontos de vigas RHS 150x100x5 de aço inoxidável 1.4301. Os modelos numéricos destes ensaios foram realizados a temperaturas elevadas, obtendo-se uma boa aproximação com os resultados experimentais. A diferença da capacidade resistente entre os resultados numéricos e os resultados experimentais é menor que 10%. São ainda utilizados métodos analíticos para previsão do comportamento força-deslocamento.

**Palavras-chave:** Resistência à flexão / Aço inoxidável / Temperaturas elevadas

## 1- INTRODUCTION

Stainless steel beams have been applied in the building industry, due to their main qualities such as high strength and ductility, good aesthetics, high corrosion resistance, and low maintenance cost. The most widely used stainless steel is the austenitic grade EN 1.4301, which usually contains a minimum of 16% chromium and 8% nickel.

Due to the increasing application of stainless-steel members in structures, considering the demand in load carrying capacity and durability, several investigations have been developed. In 1993, (Rasmussen & Hancock, 1993) presented a nonlinear method to determine deflections of stainless steel beams, based on secant and tangential modulus of elasticity. These results were compared with experimental results on 4-point bending tests, with reasonable agreement. In 2000, (Mirambell & Real, 2000) developed experimental tests on six simply supported beams loaded centrally and six continuous beams loaded symmetrically at mid-span, both experimental templates with austenitic stainless steel material. Numerical simulations were developed using beam finite elements and deflection results were also compared using the secant modulus of elasticity. Reasonable agreement was achieved for small displacements on simply supported beams. In 2004, (Gardner & Nethercot, 2004) developed a series of nine 3-point bending tests on cold-formed austenitic stainless steel beams. Full load displacement graphs were used for the validation of the numerical model and the verification of the EN1993-1-4 design rules (CEN, 2005a). These design rules are over-conservative, underpredicting the bending resistance by almost 30% for class 1 cross-section beams. The load-displacement behaviour had typical non-linear increasing and decreasing branches. The beams had almost the same slenderness range as the ones used in this paper. In 2005, (Real & Mirambell, 2005) discussed different analytical non-linear methods for the calculation of the stainless steel maximum beam deflections, presenting also numerical and experimental results. In 2006, (Gardner & Baddoo, 2006) performed experimental fire tests on four stainless steel beams to validate the numerical model applied in a parametric analysis. In 2006, (Gardner & Ng, 2006) compared the physical properties of the austenitic stainless steel with the ones from carbon steel, on the prediction of the beam temperature development under standard fire. New thermal parameters were proposed for the convection coefficient heat transfer and the emissivity of stainless steel. In 2007, (Ng & Gardner, 2007) examined previous experimental tests developed on six stainless steel beams by conducting a numerical investigation towards the prediction of the critical temperature. The ratio between the predicted and the experimental temperature was found to be around 0.74 and an improvement of 14% on the bending resistance was proposed concerning the current version of EN1993-1-2 (CEN, 2005b). Beams had similar slenderness to the ones used in our investigation. In 2010, (Lopes et al., 2010) used SAFIR to study the lateral-torsional buckling of stainless steel beams, using non-linear material and geometric models, including two modifications on SAFIR towards the constitutive law to be used for shell finite element analysis and the pattern for the residual stresses. The effect of the residual stress field is small on the ultimate load-bearing capacity of class 1 beam sections. In 2018 (Huang & Young, 2018) made a numerical investigation regarding the behaviour of lean stainless steel at elevated temperatures (from 24 to 900 °C). The results were compared with the design rules to determine the reliability and concluded that, in general, standards are conservative to predict the flexural strength at elevated temperatures. In 2019 (Pournaghshband et al., 2019) developed a

numerical investigation to determine the effect of the axial restraint on the 4-point bending behaviour of stainless steel beams under fire. A new analytical model was proposed to predict the axial restraint force (negative and positive) during the heating process, being able to model the catenary effect. Stainless steel beams are able to support higher temperatures, before the onset of the catenary effect. The numerical model was validated against carbon steel experimental tests. The numerical results were developed over twenty-one restrained and three unrestrained austenitic stainless steel beam models.

Research on stainless steel members under fire has been focusing on the development of new design formulae for beams and columns (Xing, Kucukler, et al., 2021) (Vila Real et al., 2008) (Xing, Zhao, et al., 2021), but still, there is a lack of experimental evidence of the fire resistance of stainless steel members, in particular beams at elevated temperatures.

In this experimental investigation, a set of six experimental tests on stainless steel beams were developed at elevated temperatures (500, 600 and 700 °C), showing the performance behaviour on 3-point bending setup, allowing to determine the bending resistance. A shell finite element model is developed using SAFIR (Franssen & Gernay, 2017), with two different constitutive models, based on the experimental material characterization developed by the authors in a companion manuscript (Lopes et al., 2021).

## **2- EXPERIMENTAL BENDING TEST SETUP**

### **2.1. Case study**

The test program was intended primarily to evaluate the thermal and mechanical behaviour of the steel beams at elevated temperatures. The beam specimen is subjected to a heating process to achieve constant temperature levels (500, 600 and 700 °C), then the temperature is kept constant during the incremental load application. The incremental load is based on a load rate of 66 N/s. The temperature is controlled in the furnace by one plate thermocouple, following the standard fire curve in the heating stage until the temperature level, following with a steady stage at that temperature level.

The experimental setup is based on a steel portal frame, built around the fire resistance furnace. This frame allows for the fixation of the supports used for the 3-point bending tests and is also used for the load application. The beams are positioned in the vertical direction and the load is applied by the hydraulic jack in the horizontal direction, see Fig. 1.

Four potentiometric displacement transducers are applied on the front of the load cell to measure the maximum beam displacement (D) for each load step (F). The beam has double support on the bottom and simple fork support on the top. Fig. 2 shows the materialization of the supporting conditions.

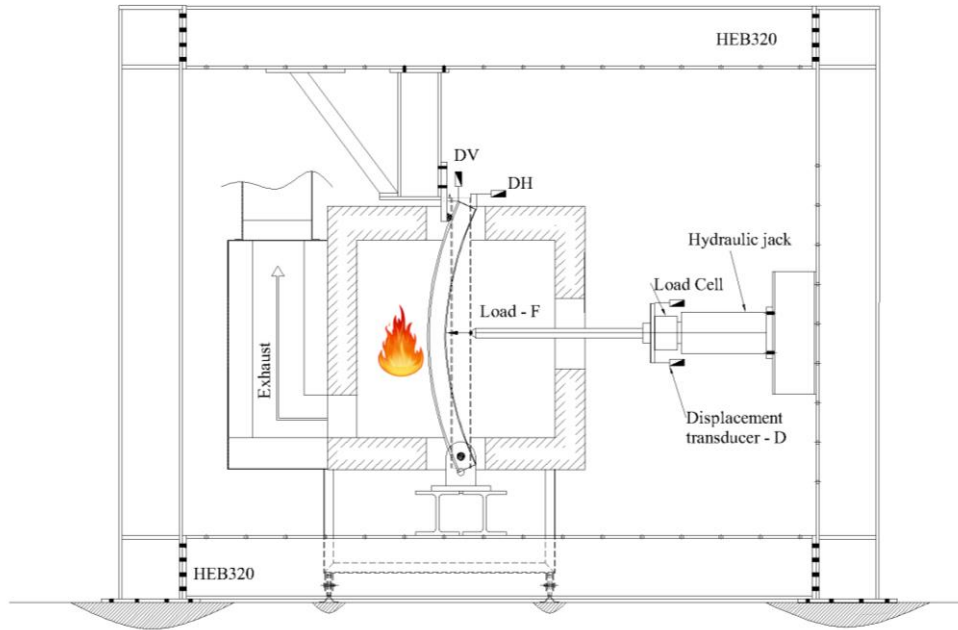


Fig. 1 | Frame, furnace and simply supported beam.



Fig. 2 | Beam inside the furnace and supporting conditions.

Load is transferred from the hydraulic jack to the beam by means of a half cylinder, distributing the load throughout the top flange, as shown in Fig. 2. There are no stiffeners applied on the load point and in the supports, hence producing the transfer of force from the flanges through the corners with consequent eccentric loading of the web of the cross-section. Both beam ends are insulated by internal parts with ceramic fibre to reduce heat loss from the internal cavity of the RHS profiles. The depth to span ratio is bigger than 8, which is enough to reproduce the beam behaviour. The same conditions are repeated two times, denoting EXP1 and EXP2.

Fig. 3 presents the geometry of the cross-section and Table 1 gives the comparison between nominal dimensions and measured dimensions, based on the average calculation of two beam elements.

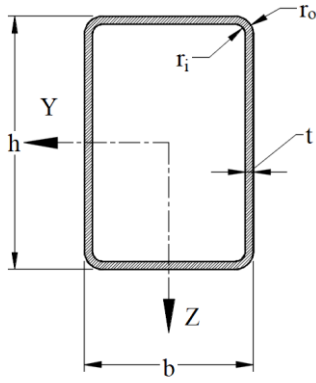


Fig. 3 | Beam cross-section.

Table 1 | RHS geometry (dimensions in mm).

Geometry	Nominal	Measured
h	150	150.35
b	100	100.35
t	5	4.78
r <sub>i</sub>	5	6.16
r <sub>o</sub>	10	10.94

A minimum of three tests were developed for the same coupon conditions for each tested profile (Lopes et al., 2021). The average results are presented in Table 2: Elastic modulus ( $E_0$ ); Proof strength ( $f_{p0.2\%}$ ); Strength at 2% strain ( $f_{p2\%}$ ); and Tensile strength ( $f_u$ ). The elastic modulus (\*) at elevated temperature was determined by the reduction factors for the slope of the linear elastic range, measured at room temperature. The reduction factors were obtained from Annex C of EN1993-1-2,  $k_{E,500} = 0.80$ ,  $k_{E,600} = 0.76$  and  $k_{E,700} = 0.71$  (CEN, 2005b).

Table 2 | Mechanical properties at elevated temperatures for the stainless steel grade 1.4301.

Temperature (°C)	$E_0$ (GPa)	$f_{p0.2\%}$ (MPa)	$f_{p2\%}$ (MPa)	$f_u$ (MPa)
20	204.84	385.82	448.68	717.38
500	163.87(*)	184.11	252.26	418.49
600	155.68(*)	170.31	227.92	350.81
700	145.44(*)	121.72	184.78	230.01

## 2.2. Instrumentation

The instrumentation consisted of four displacement transducers, as shown in Fig.1. The transducers were placed between the steel portal frame and the loading system, allowing for the measurement of the midspan deflections. The four transducers were then averaged to register the displacement D in the graphical solution. The temperature was measured by six k-type thermocouples positioned along the beam length. For each position, two thermocouples were used and averaged. Fig. 4 presents the position for every thermocouple (T1, T2 and T3). The beam span between the supports is 1.21 m and the exposed length to elevated temperature is 1 m.

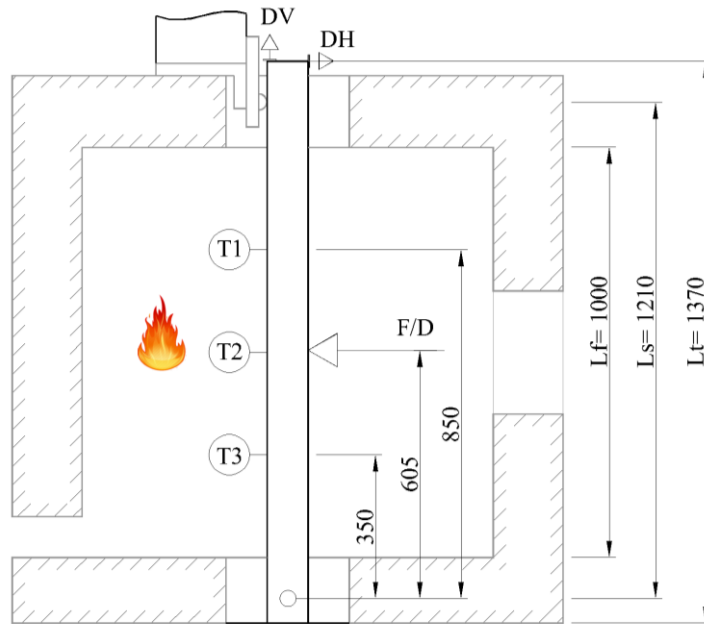
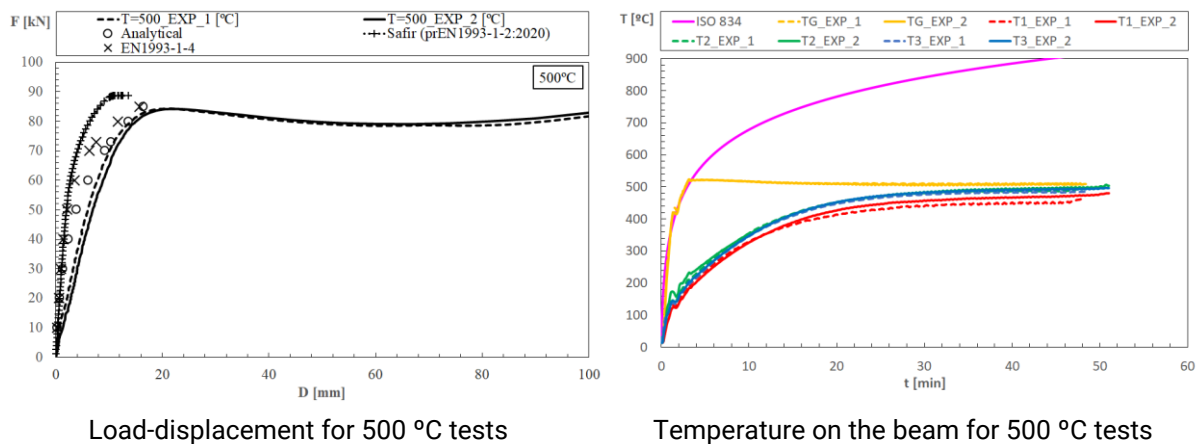


Fig. 4 | Thermocouples and position of the beam inside the furnace.

### 2.3. Test results at elevated temperature

Fig. 5 depicts the main results from the experimental tests. These results are presented for each temperature level (500, 600 and 700 °C). The load-displacement graph is typically defined by an initial increase of the load with an increase of displacement until reaching the maximum load-bearing capacity. After, the load starts to decrease with the increase of the actuator displacement. Two repetitions are represented and identified by the temperature level followed by EXP (experimental). The right side of Fig. 5 also presents the temperature evolution of each beam, with averaged values determined for sections 1, 2 and 3 (eg: T1\_EXP\_1). The furnace gas temperature (eg: TG\_EXP1) is also represented and the standard fire curve. The heating rate follows the heating rate used for the standard fire, approximately. One may conclude that temperature is almost uniform between sections 1, 2 and 3, nevertheless, a gradient is expected towards the extremities of the beams.



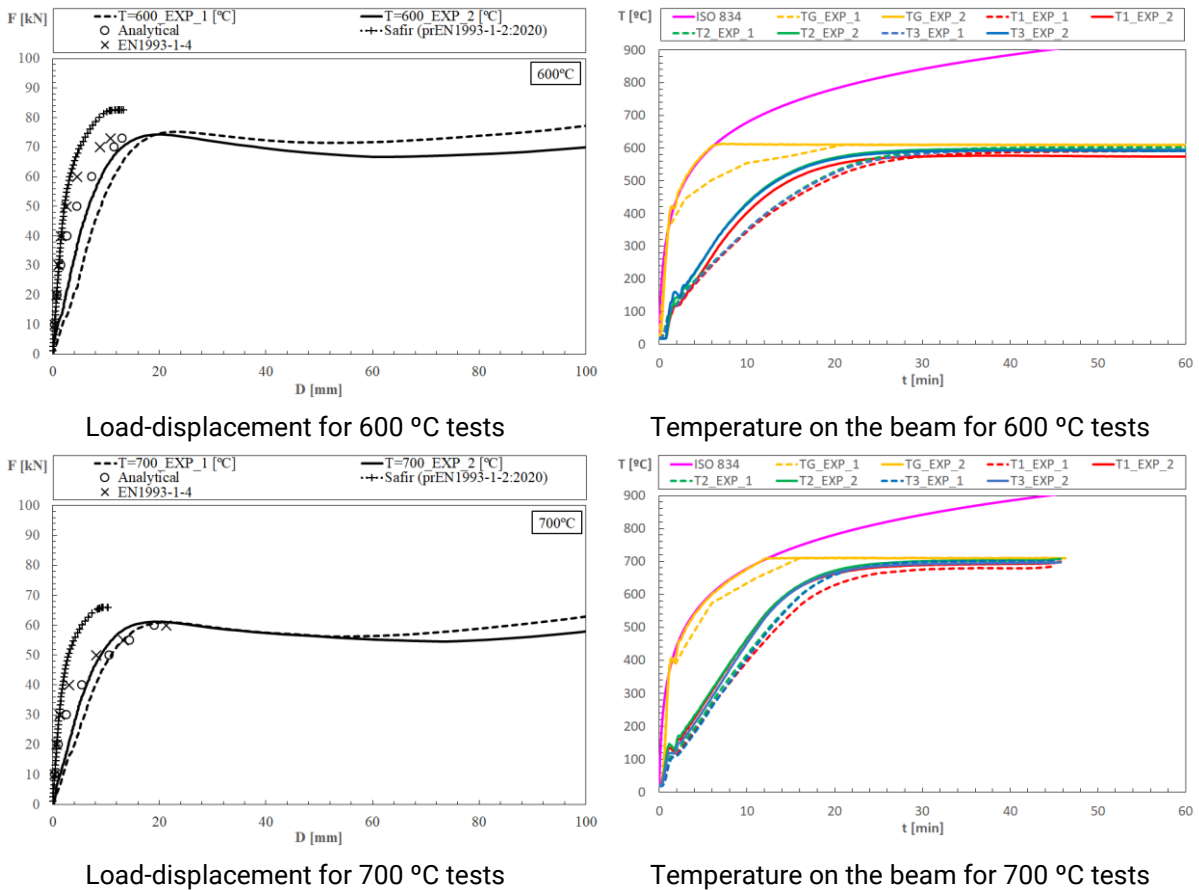


Fig. 5 | Load displacement and temperature evolution.

The load-bearing capacity is determined by the maximum peak load from the force-displacement graph (ultimate load). The deformed mode shapes included local buckling of the webs due to the loading condition (see Fig. 6). The failure mode exhibits buckling of both the compression flange and the upper portion of the web at mid-span.

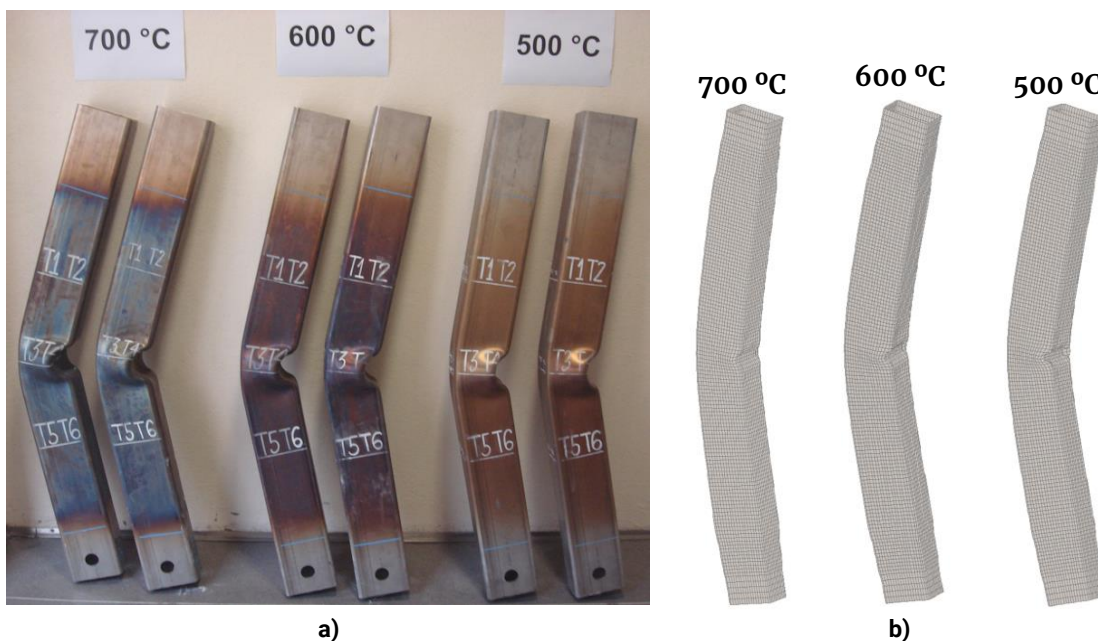


Fig. 6 | Deformed shape modes: a) experimental tests; b) numerical analysis (x10).

When comparing the load-bearing capacity with the elastic and plastic load ( $F_{el}$  and  $F_{pl}$ ), one can see that the ultimate load from the experimental tests ( $F_{u\_EXP}$ ), being  $Av\_EXP$  the average value of both tests, do not exceed the load corresponding to the plastic moment, but they exceed the elastic load, see Table 3.

**Table 3** | Comparison of the ultimate load with elastic and plastic limits.

Temp. (°C)	$F_{el}$ (kN)	$F_{pl}$ (kN)	$F_{u\_EXP}$ (kN)	$Av\_EXP$ (kN)	$F_{u\_SAFIR}$ (kN)
500	79.97	97.56	(EXP_1)=84.32; (EXP_2)=84.23	84.27	88.73
600	72.25	88.15	(EXP_1)=75.29; (EXP_2)=74.37	74.83	82.52
700	58.57	71.46	(EXP_1)=61.02; (EXP_2)=61.18	61.10	65.92

### 3- NUMERICAL VALIDATION MODEL

A three-dimensional finite element model is developed to perform geometrically and materially nonlinear numerical analyses including imperfections (GMNIA). As local buckling phenomena were likely to occur, shell finite elements were used with an initial local imperfection corresponding to 80% of the essential manufacturing tolerances. The quadrilateral shell finite element has four nodes, each with six degrees of freedom (three translations and three rotations). The membrane behaviour is approximated by a third-order polynomial, while the bending behaviour is approximated by a second order polynomial. The numerical integration is 2x2 in the plane and can change from 2 Gauss points in thickness (membrane dominated) to 10 Gauss points (bending dominated). The iterative process is verified using a tolerance of 0.001 for the out of balance forces and increments of displacement (Talamona & Franssen, 2005).

These models apply the constitutive law model proposed in the next generation (CEN, 2020), which is based on a two phase Ramberg-Osgood formulation, taking into consideration the experimental coupon test results presented in Table 2.

The solution is based on the Newton-Rapshon method, using an incremental load step of a concentrated load applied in the middle span. The nodes in the region of the applied load are coupled to have the same transversal displacement  $D$ .

The model considers the fork support in one extremity and a pinned condition applied over two nodes, to model the experimental boundary conditions of the supports.

Fig. 6 represents the deformed mode shape for each model. The deformed mode shape agrees with the experimental deformed mode. The maximum numerical load-bearing capacity approximates the maximum load of the experimental tests. The relative differences are between 5.3% at 500 °C and 10.3% at 600 °C, as shown in Table 3 ( $F_{u\_SAFIR}$ ).

## 4- ANALYTICAL METHOD FOR DEFLECTION

Deflections may be determined considering the non-linear constitutive law of stainless steel. The load-deflection curves became non-linear at low load levels. Deflections are estimated using the secant and tangent modulus and are in good agreement with experimental and numerical results. The following approximate explicit non-linear method is based on the simplified method (Rasmussen & Hancock, 1993) and is only valid for small displacements.

For any load level, the maximum bending moment  $M_{\max}$  is determined. For the case of the 3-point bending, Eq. (1) is used to determine the stress at the extreme fibre  $\sigma$ .

$$\sigma = k_{\sigma} \frac{M_{\max}}{W_e} \quad (1)$$

The factor  $k_{\sigma}$  is introduced to avoid very large deflections due to the calculation procedure to find the average secant modulus  $E_s$  at the section for the maximum bending moment and due to the calculation of the stress in the extreme fibres. This factor should be less or equal than unity ( $k_{\sigma} = 0.8$ ). The  $W_e$  represents the elastic section modulus of the cross-section. The equivalent modulus  $E_{eq}$  given by Eq. (2) is based on the average value obtained from the secant and tangent modulus from Eq. (3). These values are based on the tension and compression values for the extreme fibres at the cross-section of maximum bending moment, following the constitutive law of Ramberg-Osgood. These values were determined for each temperature level, based on the values of the experimental tensile tests, according to table 2 for the yield stress at 0.2% proof strength  $\sigma_{0.2}$  and for the elastic modulus  $E_0$ . The constant value of 3.56 is used for the parameter  $n$  (Rasmussen & Hancock, 1993).

$$E_{eq} = (E_s + E_T) / 2 \quad (2)$$

$$E_s = \left[ 1 + 0.002 \frac{E_0}{\sigma_{0.2}} \left( \frac{\sigma}{\sigma_{0.2}} \right)^{n-1} \right]^{-1} \times E_0 \quad \text{and} \quad E_T = \left[ 1 + 0.002 \times n \times \frac{E_0}{\sigma_{0.2}} \left( \frac{\sigma}{\sigma_{0.2}} \right)^{n-1} \right]^{-1} \times E_0 \quad (3)$$

The maximum deflection is then calculated according to Eq. (4), replacing the Elastic modulus  $E_0$ , with the equivalent elastic modulus  $E_{eq}$ .

$$D = \frac{PL^3}{48E_{eq}I} \quad (4)$$

The results for the load-deflection are presented in Fig 5. for different load levels and for each temperature level. The results agree very well with the numerical and experimental results.

A similar approximation is presented for the current version of EN1993-1-4 (CEN, 2005a) using only the secant modulus of elasticity, as an average between the value determined for the compression and tension flanges. The values for the secant modulus may be estimated using Eq. (5), where  $\sigma_{i,Ed,ser}$  represents the serviceability design stress,  $f_y$  the yield stress and the parameter  $n$  depends on the grade of the stainless steel (in this case  $n = 6$ ).

$$E_s = \frac{E_0}{\left[ 1 + 0.002 \frac{E_0}{\sigma_{i,Ed,ser}} \left( \frac{\sigma_{i,Ed,ser}}{f_y} \right)^n \right]} \quad (5)$$

### 3. CONCLUSIONS

This experimental investigation considers six experimental bending tests of 1.4301 austenitic stainless steel beams, made with RHS 150x100x5 cross-section. The beams are tested at three different temperature levels (500, 600 and 700 °C). The ultimate load for each beam (load-bearing) is compared with the expected elastic and plastic behaviour. The results are also compared with the SAFIR numerical model, considering the constitutive law from the next generation of the EN1993-1-2. The modified analytical method is also presented to determine the load-displacement behaviour of these beams at elevated temperatures.

### ACKNOWLEDGEMENT

Part of this research work was performed within the framework of the project "StaSteFi - Fire design of stainless steel members", PTDC/ECI-EGC/30655/2017, supported by the Portuguese Operational Programme "Competitividade e Internacionalização", in its FEDER/FNR component, and the Portuguese Foundation for Science and Technology (FCT), in its State Budget component (OE).

### REFERÊNCIAS

- CEN. (2005a). EN 1993-1-4:2006 - Eurocode 3: Design of steel structures - Part 1-4: General rules - Supplementary rules for stainless steels. In *CEN- European Committee for Standardization*. CEN.
- CEN. (2005b). EN1993-1.2: 2005 - Eurocode 3: Design of steel structures - Part 1-2: General rules - Structural fire design. In *CEN- European Committee for Standardization*. <https://doi.org/10.4324/9781315780320-29>
- CEN. (2020). prEN1993-1.2: 2020 - Eurocode 3: Design of steel structures - Part 1-2: General rules - Structural fire design. In *CEN- European Committee for Standardization*. CEN.
- Franssen, J. M., & Gernay, T. (2017). Modeling structures in fire with SAFIR®: Theoretical background and capabilities. *Journal of Structural Fire Engineering*, 8(3), 300-323. <https://doi.org/10.1108/JSFE-07-2016-0010>
- Gardner, L., & Baddoo, N. R. (2006). Fire testing and design of stainless steel structures. *Journal of Constructional Steel Research*, 62(6), 532-543. <https://doi.org/10.1016/j.jcsr.2005.09.009>
- Gardner, L., & Nethercot, D. A. (2004). Experiments on stainless steel hollow sections-Part 2: Member behaviour of columns and beams. *Journal of Constructional Steel Research*, 60(9), 1319-1332. <https://doi.org/10.1016/j.jcsr.2003.11.007>

- Gardner, L., & Ng, K. T. (2006). Temperature development in structural stainless steel sections exposed to fire. *Fire Safety Journal*, 41(3), 185–203. <https://doi.org/10.1016/j.firesaf.2005.11.009>
- Huang, Y., & Young, B. (2018). Structural performance of cold-formed lean duplex stainless steel beams at elevated temperatures. *Thin-Walled Structures*, 129(February), 20–27. <https://doi.org/10.1016/j.tws.2018.03.031>
- Lopes, N., Real, P. V., da Silva, L. S., & Franssen, J. M. (2010). Numerical modelling of thin-walled stainless steel structural elements in case of fire. *Fire Technology*, 46(1), 91–108. <https://doi.org/10.1007/s10694-009-0084-x>
- Mirambell, E., & Real, E. (2000). On the calculation of deflections in structural stainless steel beams: An experimental and numerical investigation. *Journal of Constructional Steel Research*, 54(1), 109–133. [https://doi.org/10.1016/S0143-974X\(99\)00051-6](https://doi.org/10.1016/S0143-974X(99)00051-6)
- Ng, K. T., & Gardner, L. (2007). Buckling of stainless steel columns and beams in fire. *Engineering Structures*, 29(5), 717–730. <https://doi.org/10.1016/j.engstruct.2006.06.014>
- Nuno Lopes, Arrais, F., Real, P. V., Alves, M., Mesquita, L., & Piloto, P. (2021). Resistência mecânica de elementos em aço inoxidável a temperaturas elevadas. *12th Portuguese Congress on Experimental Mechanics (CNME2020)*.
- Pournaghshband, A., Afshan, S., & Theofanous, M. (2019). Elevated temperature performance of restrained stainless steel beams. *Structures*, 22(September), 278–290. <https://doi.org/10.1016/j.istruc.2019.08.015>
- Rasmussen, K. J. R., & Hancock, G. J. (1993). Design of Cold-Formed Stainless Steel Tubular Members. II: Beams. *Journal of Structural Engineering*, 119(8), 2368–2386. [https://doi.org/10.1061/\(ASCE\)0733-9445\(1993\)119:8\(2368\)](https://doi.org/10.1061/(ASCE)0733-9445(1993)119:8(2368))
- Real, E., & Mirambell, E. (2005). Flexural behaviour of stainless steel beams. *Engineering Structures*, 27(10), 1465–1475. <https://doi.org/10.1016/j.engstruct.2005.04.008>
- Talamona, D., & Franssen, J. M. (2005). A Quadrangular Shell Finite Element for Concrete and Steel Structures Subjected to Fire. *Journal of Fire Protection Engineering*, 15(4), 237–264. <https://doi.org/10.1177/1042391505052769>
- Vila Real, P. M. M., Lopes, N., Simões da Silva, L., & Franssen, J. M. (2008). Lateral-torsional buckling of stainless steel I-beams in case of fire. *Journal of Constructional Steel Research*, 64(11), 1302–1309. <https://doi.org/10.1016/j.jcsr.2008.04.013>
- Xing, Z., Kucukler, M., & Gardner, L. (2021). Local buckling of stainless steel I-sections in fire: Finite element modelling and design. *Thin-Walled Structures*, 161(January), 107486. <https://doi.org/10.1016/j.tws.2021.107486>
- Xing, Z., Zhao, O., Kucukler, M., & Gardner, L. (2021). Testing of stainless steel I-section columns in fire. *Engineering Structures*, 227(November 2020). <https://doi.org/10.1016/j.engstruct.2020.111320>